Spectroscopy of the O-H and O-D stretching vibrations in $SrTiO_3$ under applied electric field and uniaxial stress

G. Weber, S. Kapphan,* and M. Wöhlecke
University of Osnabrück, FB Physik, P.O.B. 4469, D-4500 Osnabrück, Federal Republic of Germany
(Received 27 May 1986)

High-resolution measurements of the ir stretching bands of OH and OD at about 3500 cm^{-1} and 2600 cm^{-1} in monodomain $SrTiO_3$ crystals yield spectroscopic data for a local anharmonic-oscillator model. The optical polarization dependence and the splitting of the absorption bands at low temperature under applied electric field and uniaxial stress give additional evidence for three sets of local oscillators proposed earlier [S. Kapphan, J. Koppitz, and G. Weber, Ferroelectrics 25, 585 (1980)], one being polarized completely perpendicular and the other two forming an angle of 45° with the tetragonal c axis. The main O-H and O-D lines have also been found in Raman spectroscopy displaying the same general behavior and splitting into three components below the structural phase-transition temperature. The above results support the model assuming localized O-H oscillators at regular oxygen lattice sites with the O-H stretching vibration along the oxygen-oxygen directions.

I. INTRODUCTION

Hydrogen impurities have been the subject of many recent investigations in oxidic material, because of their presence in most as grown crystals and their influence on physical properties useful for device applications. In $LiNbO_3$ hydrogen appears to play a prominent role in waveguides produced by proton exchange and titanium in-diffusion.[1,2] For instance, the mobile ions, which neutralize the electronic space-charge field during the thermal fixing of volume holograms in $LiNbO_3$:Fe have been identified to be protons[3] and the laser optical damage seems to be favorably diminished in the presence of hydrogen in these crystals.[1,4] The OH-group second-overtone absorption, on the other hand, is limiting the performance of many optical fibers and therefore hydrogen is studied intensively in SiO_2 products.[5–9] In potassium titanate orthophosphate the presence of hydrogen reduces the nonlinear polarizability as seen by second-harmonic generation.[10] In MgO and Al_2O_3 hydrogen is found to influence the luminescence in thermochemically reduced samples thereby affecting adversely their properties as active materials for tunable lasers.[11,12]

Diffusion studies of OH, OD, and OT in materials[13–19] such as TiO_2, Al_2O_3, $KTaO_3$, and $LiNbO_3$ at elevated temperatures did yield diffusion coefficients and activation energies. However, very little conclusive evidence about the possible sites of hydrogen in the oxidic lattices has been reported. The infrared optical properties of oxides containing hydrogen and its isotopes provide not only a convenient means of estimating the concentration of OH, but also allow one to study the interaction of hydrogen with neighboring ions in some more detail. The O-H stretching vibration exhibits a change of the electric dipole moment along the molecular axis and thus the ir absorption of a single molecule is linearly polarized. The axial symmetry of the free molecule is lowered to the symmetry of the site in the host, reflecting the local environment. Therefore the ir absorption is an adequate tool to study the change of the environment induced by phase transitions and the influence of external electric fields and stress.

This is of particular interest for $SrTiO_3$ with its prototype structural (antiferrodistortive) phase transition at about 105 K. Several studies have examined the temperature dependence of the relative sharp O-H absorption peaks[20] and their splitting into three components below the phase-transition temperature.[21–24] Limited spectral resolution and partly polydomain samples used in some of the earlier studies led to conflicting discussions about the actual sites for hydrogen in $SrTiO_3$,[22–24] and a coupling to the ferroelectric zone center mode.[23,24] We therefore investigated the O-H and O-D vibrations in monodomain $SrTiO_3$ samples with improved resolution under the influence of external electric fields and uniaxial stress. Preliminary measurements of the spectroscopic data close to the phase transition and first results on the electric field dependence have been published previously.[22] Here new experimental data on both field- and stress-induced properties as well as first results on Raman scattering of the hydrogen centers are reported. The field-induced splitting of the vibrational modes yields new and detailed information about the vibrational directions of the hydrogen impurities. The results favor a model for the hydrogen sites close to oxygen lattice sites with the O-H vibrating in direction of the next-nearest oxygen ion.

II. EXPERIMENTAL CONSIDERATIONS

A. Samples

The crystals used in our investigations have been grown by two different growth techniques, the Verneuil and the Czochralski methods. They were obtained from different crystal-growth laboratories.[25,26] This variety of samples of different origins and growth processes allows one to find out common spectroscopic features. The samples studied are rectangular-shaped slabs of about $5\times10\times5$

mm^3 cut from as grown crystals and polished. All crystallographic axes are given with respect to cubic axes.

Nominally pure single crystals show a low hydrogen content. Typical figures of the absorption coefficients are of the order of 1 cm^{-1}. In order to raise this value and to study the variation of the spectroscopic properties on the hydrogen content, the crystals have been doped, using a hydrothermal pressure technique.[27] Doping with H_2O or D_2O vapor at high pressure and a temperature of about 800 K results in an increase of the absorption coefficient of the stretching vibration up to values of 8 cm^{-1}. In addition we want to point out that doping with D_2O (or H_2O) vapor allows a nearly complete exchange of hydrogen against deuterium.

B. Apparatus

The infrared spectra were obtained using a Bruker rapid-scan Fourier ir spectrometer (IFS 113 Cv) with a resolution better than 0.1 cm^{-1}. In order to guarantee a signal-to-noise ratio of better than 10^3, the spectral range has been limited by means of suitable optical bandpass filters. A liquid-nitrogen-cooled InSb detector was used. Linear polarized light was achieved by Perkin Elmer wire-grid polarizers.

The experiments were performed in an exchange-gas helium cryostat with an absolute temperature accuracy of ± 0.5 K and a relative temperature stability of ± 0.1 K. External electric fields and uniaxial stress are applied by means of well known techniques.[28,29] For the absorption spectra with a light beam ($\mathbf{k}_L$) parallel to the external electric field, Ni nets (4×10^{-5} m width of mesh) with 50% transmission were used. Absolute figures for both the electric field and stress are given with an uncertainty of 5%. This is due to minor irregularities of the crystal-net contact and small friction of the stress piston at low temperatures.

Right-angle Raman scattering experiments have been performed using a double Spex 1400 spectrometer with holographic gratings and conventional photon-counting techniques.

III. INFRARED SPECTRA AND THEIR ANALYSIS

A. Room-temperature spectra

A free diatomic O-H oscillator can be excited by light only, which has electric field components parallel to the molecule axis. This holds for a single dipole in a solid, too. Governed by the symmetry group of the crystal, there exist several energetically equivalent positions for the diatomic oscillator. Therefore in cubic crystals such as $SrTiO_3$ at room temperature an isotropic absorption is expected and indeed found.

In crystals of different origin the main absorption line due to a O-H (O-D) stretching appears at room temperature at $\nu(\mathrm{OH})=3495.4$ cm^{-1} ($\nu(\mathrm{OD})=2581.6$ cm^{-1}) with a full width at half maximum (FWHM) of $\Delta\nu(\mathrm{OH})=2.6$ cm^{-1} and $\Delta\nu(\mathrm{OD})=1.9$ cm^{-1}, respectively. Thus within experimental scattering the relative half-widths (FWHM) are $\Delta\nu/\nu=7.4\times10^{-4}$ for both O-H and O-D vibrations. The hydrogen (deuterium) content can be estimated to be

$$n(\mathrm{H})\approx(7.0\times10^{16}\ \mathrm{cm}^{-2})\alpha_{\max}(\mathrm{OH})$$

$$n(\mathrm{D})\approx(0.95\times10^{16}\ \mathrm{cm}^{-2})\alpha_{\max}(\mathrm{OD})$$

using the oscillator strength of the appropriate stretching vibration in TiO_2.[13] $\alpha_{\max}(\mathrm{OH})$ and $\alpha_{\max}(\mathrm{OD})$ are the maximum of the corresponding absorption lines in cm^{-1}.

Beside the main absorption line, some samples show weak additional structure at both higher and lower energies compared to the main bands. However, their intensity ratios with the main band vary, presumably depending on the chemical purity of the samples. Figure 1 shows the room-temperature spectra of the O-H stretching vibrations of three different crystals. The central spectrum consists of only one line caused by the O-H stretching vibration and represents one extreme case of our investigations. The bottom spectrum exhibits another extreme case, because several additional structures are seen. The peak positions are despite of a general shift of about 1 cm^{-1} almost identical with those in references.[23,24] Most of the shift is easily explained by the use of vacuum wave numbers in our case. A typical result is shown with the spectrum at the top of Fig. 1. Only a few additional structures are seen on the high-energy side of the stretching vibration. We have shown that the additional high-energy lines are closely related to hydrogen, because they grew in a similar manner as the main band as observed with controlled doping experiments. Supplementary broad structures with half-widths of 10–20 cm^{-1} have been seen on the low-energy side (2850–3380 cm^{-1}) of the main line. Because no clear correspondence with the hydrogen content could be established, we exclude this part of the spectrum in further discussions.

B. Overtone spectroscopy

Valuable information may be gained from the detection of the first overtone of the stretching vibration. Figure 2 shows the spectra of the first overtone for the O-H and O-D stretching vibration at room temperature. The appearance of the overtone at a wave number 6816 cm^{-1} (5073 cm^{-1}) almost twice that of the fundamental mode and its small linewidth of 7.5 cm^{-1} (6 cm^{-1}) indicates a

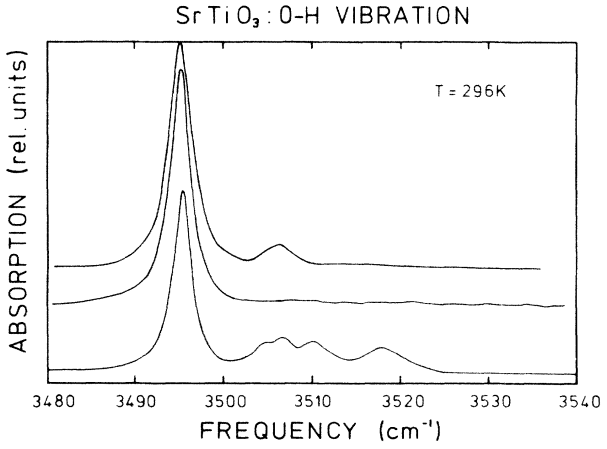

FIG. 1. Absorption spectra of three different $SrTiO_3$ samples doped with hydrogen.

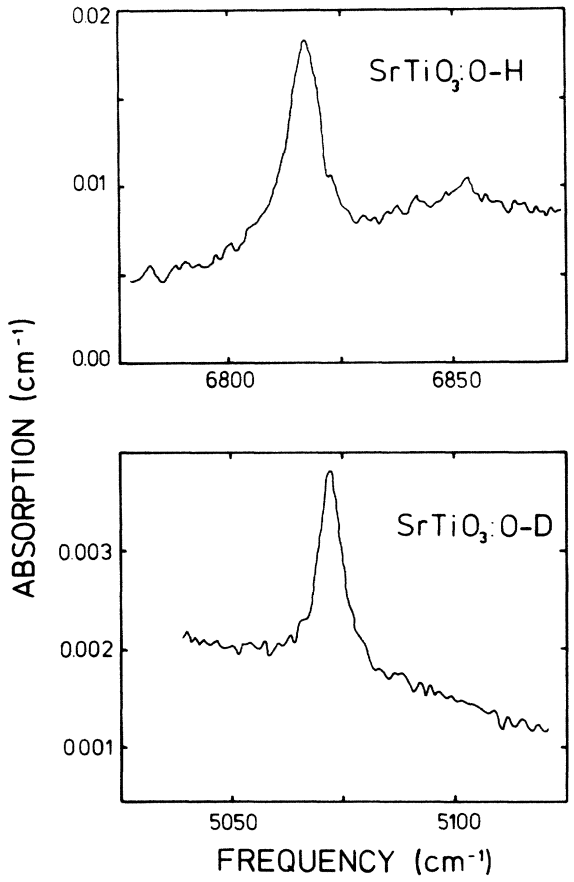

FIG. 2. First overtone of the O-H and O-D stretching vibration in $SrTiO_3$.

local mode with a deep potential and little anharmonicity.

This is supported by the isotope shift of $\nu(\mathrm{OH})/\nu(\mathrm{OD})=1.354$ which is comparable to that of KBr:OH(OD),[30] and is very close to the value $\mu(\mathrm{OH})/\mu(\mathrm{OD})=1.374$ expected for a local mode with reduced mass μ.

We can also use the ratio of the intensity of the stretching vibration $I(0,1)$ and its first overtone $I(0,2)$ to draw more conclusions on the nature of the vibrating molecule. The intensity ratio $I(0,2)/I(0,1)$ is found experimentally to be

$$\frac{I(0,2)}{I(0,1)}=\frac{\alpha(0,2)\Delta\nu(0,2)}{\alpha(0,1)\Delta\nu(0,1)}=(1.0\pm0.2)\times10^{-2}$$

for O-H vibrations and $(1.3\pm0.2)\times10^{-2}$ for O-D stretching modes. The figures in parentheses indicate the vibrational quantum numbers, see Sec. III D.

This ratio has been calculated[31] with respect to the molecular dipole moment $p=p_0+p_1x+p_2x^2$. For a linear dependence of p on the elongation that means $p_2/p_1=0$, a value of 2.5×10^{-2} was obtained. This reduces to 0.8×10^{-2} in the case of a nonlinear dependence ($p_2/p_1=-0.5$) and is close to the experimental finding. According to calculations on the OH molecule in neutral and ionized states, the neutral molecule possesses a linear dependence of the dipole moment on the displacement, while the OH^- molecule requires a nonlinear one.[32] Thus we have evidence for the existence of OH^- molecules in $SrTiO_3$.

C. Temperature dependence

While lowering the temperature below $T_0=105$ K, the main line splits into three components $\nu_A<\nu_B<\nu_C$ (Fig. 3) reflecting the cubic to tetragonal structural phase transition. The temperature dependence of the frequency of the dominant local oscillator is that reported previously by several groups.[21–24] In the cubic phase both the frequency and the crystal volume depend linearly on the temperature. For 70 K$<T<T_0=105$ K the square of the energy splitting $\nu_C-\nu_A$ is proportional to the difference $T-T_0$. This is the temperature dependence of the order parameter, the rotation angle of the oxygen octahedron.[33,34] The phase transition temperature T_0 has been found with a sample dependent scatter of ±2 K to be $T_0=105$ K by means of an extrapolation of $(\nu_C-\nu_A)^2$ to zero splitting. Outside the sample dependent variation of 2 K no dependence of T_0 on the hydrogen content has been found. The relative linewidth reduces from 7.4×10^{-4} at room temperature to 1.3×10^{-4} at 120 K and at helium temperature. Close to T_0 a broadening of the linewidth is observed.

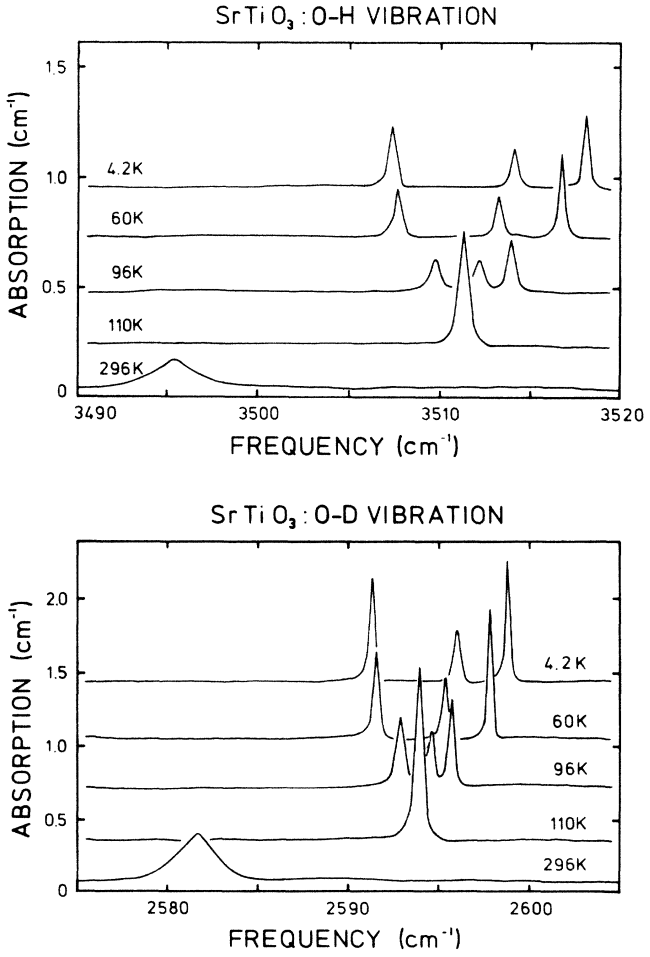

FIG. 3. O-H and O-D absorption spectra at different temperatures. The spectra are shifted for better viewing.

The weak bands at higher energies shift with lowered temperatures in the same manner as the main line and most of them split in an analogous pattern. The intensity ratio of these bands with that of the main line is nearly temperature independent. The assumption that the weak bands are due to O-H vibrations perturbed by other defects in the vicinity of the hydrogen impurity can account for this temperature independent fixed intensity ratio and the energetic shift parallel to the dominant band.

None of the satellite bands exhibit a temperature dependence analogous to that of the "ferroelectric" soft mode. Therefore both the temperature dependence and the variation of the side bands from sample to sample (see Fig. 1) cast doubt on the proposal[24] of their origin being due to a coupling to ferroelectric and antiferrodistortive mode fluctuations. In the following we will limit our discussion to the behavior of the main O-H and O-D stretching band.

Below T_0, $SrTiO_3$ becomes tetragonal due to a rotation of the oxygen octahedra and a doubling of the unit cell. Usually three orthogonal domain directions appear with equal probability. It has been shown that under moderate uniaxial stress in a $\langle 110 \rangle$ direction a monodomain sample with the tetragonal c axis parallel to the cubic $\langle 001 \rangle$ axis results.[35] Therefore the crystal is no longer isotropic with respect to the absorption of linear polarized light. Because the stretching vibration can only be excited by linear polarized light with an electric field vector $\mathbf{E}_L$ parallel to the dipole axis, pronounced dependence of the absorption on the direction of E_L is expected. Preliminary data with limited spectral resolution for O-H bands in monodomain samples have been published previously[22] by us, in particular spectroscopic data close to the phase transition and preliminary measurements on the electric field dependence. New experimental data with improved resolution using polarized light are presented in Fig. 4 and clearly demonstrate the strong polarization behavior of the stretching mode. For light with $\mathbf{E}_L \| [110]$, all the absorption lines are seen with the center line dominating in intensity. This changes drastically for $\mathbf{E}_L \| [001]$, with light polarized parallel to the tetragonal c axis. Here the center line of the triplet disappears for both O-H and O-D, whereas the outer components are seen with an intensity increased by a factor of 2. Therefore the center line ν_B corresponds to dipoles lying in the xy plane, while the outer components ν_A and ν_C must have displacement components parallel to the tetragonal axis.

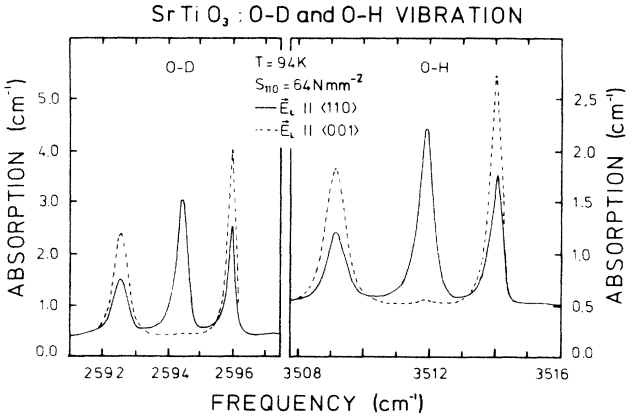

FIG. 4. Polarization dependence of the O-H and O-D dominant lines below T_0 in a monodomain crystal (S_{110} stress).

D. Spectroscopic constants

In the preceding section we have pointed out that weak anharmonic effects have to be considered to understand the excitation energies. Therefore we have applied the model of a local anharmonic diatomic oscillator to describe the stretching vibrations. A realistic and often used potential is the Morse potential

$$V(x)=D[1-\exp(-ax)]^2 \tag{3.1}$$

with $x=r-r_e$. D is the depth of the potential energy minimum and represents the bond dissociation energy, the energy required to separate the two ions from their equilibrium distance r_e to infinite separation. Solving the Schrödinger equation, the constant a and the energies in reciprocal centimeters for the levels $G(v)$ with vibrational quantum number v are given by[36,37]

$$G(v)=\omega_e(v+\tfrac{1}{2})-\omega_e x_e(v+\tfrac{1}{2})^2 \tag{3.2}$$

with

$$\omega_e=(a/2\pi c)(2D/\mu)^{1/2} \tag{3.3a}$$

and

$$x_e=hc\omega_e/4D\ . \tag{3.3b}$$

The quantity $x_e\omega_e$ is known as the anharmonicity constant. In the above equation h is Planck's constant, c is the speed of light, and μ is the reduced mass.

Substitution of the hydrogen ion of the diatomic OH molecule by deuterium of mass m_i results in a molecule of reduced mass μ_i equal to $m_i m_0/(m_i+m_0)$ with m_0, the mass of oxygen. With the use of $\rho_i=(\mu/\mu_i)^{1/2}$ the energy levels now read[37]

$$G_i(v)=\rho_i\omega_e(v+\tfrac{1}{2})-\rho_i^2\omega_e x_e(v+\tfrac{1}{2})^2\ . \tag{3.4}$$

From this equation we derive the expressions for transitions from $v=0$ to $v=1$ and $v=2$:

$$\nu_i(0,1)=G_i(1)-G_i(0)=\rho_i\omega_e-2\rho_i^2\omega_e x_e\ , \tag{3.5}$$

$$\nu_i(0,2)=G_i(2)-G_i(0)=2(\rho_i\omega_e-3\rho_i^2\omega_e x_e)\ . \tag{3.6}$$

The isotope shift and the first overtone offer two independent ways to determine the spectroscopic parameters from the experimental data tabulated in Table I. We start with the isotope shift at room temperature and obtain from Eqs. (3.3a), (3.3b), and (3.5), a frequency $\omega_e=3688$ cm^{-1}, an anharmonicity constant $\omega_e x_e=96.7$ cm^{-1} and a dissociation energy $D=4.36$ eV. These values are presented together with those for lower temperatures in Table II. A second set of parameters follow for room temperature from the energy of the first overtone according to Eqs. (3.3a), (3.3b), (3.5), and (3.6) and has been included in Table II. The figures calculated agree with ω_e within 1%, while for $x_e\omega_e$ and D a variation of about 10% was found.

TABLE I. Experimental data of the O-H and O-D stretching vibrations in $SrTiO_3$. In column three the expression 2:1 gives the intensity ratio of the absorption line for light vector $\mathbf{E}_L \| c$ to $\mathbf{E}_L \perp c$. If no figure is given, the line is completely polarized with respect to the c axis.

			O-H vibration			O-D vibration		
Temp. T (K)	Absorption band	Polarization	Energy (cm^{-1}) $\nu(0,1)$	FWHM $\Delta\nu$ (cm^{-1})	Energy (cm^{-1}) $\nu(0,2)$	Energy ν (cm^{-1})	FWHM $\Delta\nu$ (cm^{-1})	Energy (cm^{-1}) $\nu(0,2)$
300	$A=B=C$	Isotropic	3495.4	2.6	6816	2581.6	1.9	5073
120	$A=B=C$	Isotropic	3510.4	0.5		2593.4	0.35	
94	A	2:1$\|\|C$	3509.6	0.7		2592.9	0.5	
	B	only$\perp C$	3512.1	0.6		2594.6	0.45	
	C	2:1$\|\|C$	3513.9	0.45		2595.9	0.35	
4.2	A	2:1$\|\|C$	3507.4	0.4		2591.5	0.3	
	B	only $\perp C$	3514.2	0.35		2596.1	0.25	
	C	2:1$\|\|C$	3518.1	0.3		2598.9	0.23	
	Uncertainty		±0.2	±0.05	±1	±0.2	±0.05	±1

The isotope shift and the first overtone probe the potential in different manner. The isotope shift reflects the lower part behavior of the oscillator potential, which should be similar in other ABO_3 compounds with stretching vibrations of small linewidth. This assumption is supported by the dissociation energies of about 4.3 eV and anharmonicity constants of (96±3) cm^{-1} found also in the case of $KTaO_3$:H and $BaTiO_3$:H.[18,38] The parameters determined from the first overtone are more sensitive to anharmonic terms in the potential, because the ionic displacements are larger. For example, for the free OH ion an anharmonicity constant $x_e\omega_e = 87.8$ cm^{-1} has been calculated with an uncertainty of 10%.[32] Our values are close to this estimate and together with a very small half-width (FWHM) of the lines indicate a weak interaction of the local O-H oscillator with the host lattice. This is quite different for TiO_2 and Al_2O_3, where larger bandwidths indicate a stronger coupling to the host lattice and thus larger values for $\omega_e x_e$ are reported.[14,17]

For the discussion in IV C we present here the expressions for an anharmonic oscillator in an external electric field. To obtain the potential energy a term $Eq(x+r_e)$ has to be added to (3.1). With the condition $V'(x_0)=0$ and

$$\omega_e(E) = \frac{1}{2\pi c}\left[\frac{V''(x_0)}{\mu}\right], \tag{3.7}$$

we obtain the frequency

$$\omega_e(E) \approx \omega_e(E=0)\left[1-\frac{3qE}{4aD}\right], \tag{3.8}$$

for $3q/4aD \ll 1$. From this we calculate

$$\nu(0,1)(E) = \omega_e(E)(1-2x_e)\ . \tag{3.9}$$

With the assumption of an electric field independent quantity x_e, the frequency shift between a dipole parallel and antiparallel to the field is given by

$$\frac{\Delta\nu(0,1)}{\nu(0,1)}(E) = \frac{3}{2}\frac{Eq}{aD} = \alpha E\ . \tag{3.10}$$

Here E is the local field and α can be expressed in the form

$$\alpha = \frac{3q}{2\pi}\left[\frac{2\omega_e x_e}{\mu h c^3 \omega_e^4}\right] \tag{3.11}$$

and evaluated with the parameters presented in Table II.

E. Raman spectra

In addition to the infrared spectra we have investigated the Raman spectra of the O-D and O-H stretching vibrations. Results are shown for room temperature and for $T < T_c$ in Fig. 5. We achieved typical count rates of a few counts/sec using a focussed beam of the Ar 488-nm line with a power of 3 W. Each data point represents an

TABLE II. Spectroscopic parameters of the O-H and O-D stretching vibrations in $SrTiO_3$.

	Isotope shift			O-H overtone			O-D overtone		
Temp. T (K)	ω_e (cm^{-1})	$x_e\omega_e$ (cm^{-1})	D (eV)	ω_e (cm^{-1})	$x_e\omega_e$ (cm^{-1})	D (eV)	ω_e (cm^{-1})	$x_e\omega_e$ (cm^{-1})	D (eV)
300	3681.6	93.1	4.5	3669	87	4.8	2672	45	4.9
120	3701.0	95.3	4.4						
94	3700.6	95.5	4.4						
	3702.5	95.2	4.5						
	3704.2	95.2	4.5						
4.2	3699.4	96.0	4.4						
	3704.4	95.1	4.5						
	3708.1	95.0	4.5						

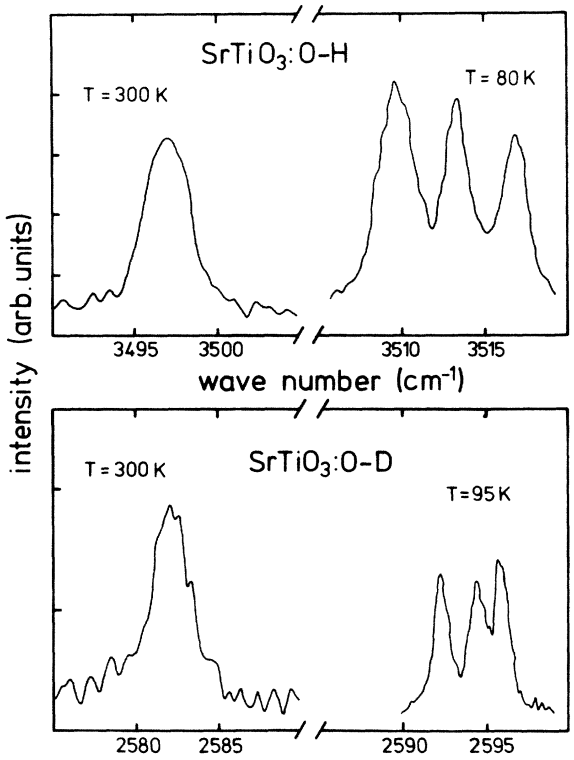

FIG. 5. Unpolarized Raman scattering of the stretching vibration at room temperature and below T_0.

integration of 100 sec obtained in 10 scans. For room temperature, the band pass of the spectrometer is comparable to the half-width of the infrared bands (see Table I), while for $T < T_c$ the resolution is limited by the instrument. For both O-D and O-H the room temperature spectrum exhibit a single line. At temperatures $T < T_c$ a splitting in a triplet is observed. The splitting and temperature dependence of the Raman lines show a behavior in complete analogy with the infrared absorption. The observation of three Raman lines of nearly equal strength is in full agreement with the octahedron model discussed above. More details will be discussed in a forthcoming publication.[39]

IV. MODELS FOR THE HYDROGEN SITE AND ENERGY SPLITTING BY EXTERNAL PERTURBATIONS

A. O-H site models

The energy of the O-H stretching mode is about 60 cm^{-1} lower than that of the free molecule, measured recently.[40] Such small shifts combined with a small half-width of the absorption line at room temperature are common to other ABO_3 compounds such as $KTaO_3$ (Ref. 18) and $BaTiO_3$.[41] Because of the small linewidth we rule out a hydrogen bridge bond in a $OH \cdots O$ configuration, but follow the assumption of hydrogen vibrating in direction of the O—O bond proposed in (Ref. 21). In $SrTiO_3$ there are two possibilities to place hydrogen between oxygen ions. We will in the following call this proposal of hydrogen vibrating along the O—O bonds the octahedron model.

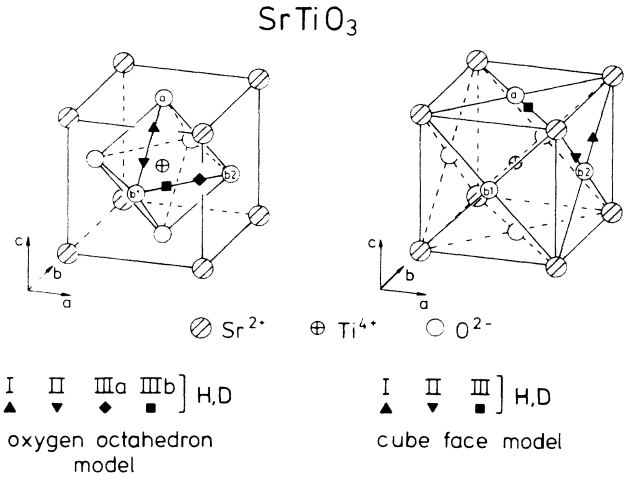

FIG. 6. Octahedron model and the cube face model.

Another model, which places the hydrogen between oxygen ions has been proposed by Brebner *et al.*[23] Here the hydrogen is assumed to be placed in direction of nearest-neighbor (NN) oxygen ions along the cubic axes. First, the oxygen distance of about 4 Å gives no motivation for such a model and second, none of the absorption bands with polarization parallel the tetragonal c axis as required by this axial site model has been observed. Therefore this model is omitted. A third version has been introduced by the same group.[24] This model places the hydrogen on the faces of the cube, between the oxygen and the strontium atoms.

The octahedron model and the cube face model are shown in Fig. 6 for comparison. Above T_0, in the cubic phase, all sites are degenerate with respect to energy, predicting one frequency as observed. This is altered for $T < T_0$ where adjacent octahedra rotate in reverse sense. The unit cell obtained has doubled lattice constants and is different from the conventional unit cell in tetragonal systems.

We start with the octahedron model. First we consider the two different sites I and II, which are on the edges of the octahedron, but not in the a,b plane. These positions are assumed to cause the two outer components with the predicted and observed intensity ratio 2:1 for $\mathbf{E}_L \| c$ and $\mathbf{E}_L \perp c$. Sites IIIa and IIIb are responsible for the absorption peaks completely polarized with $\mathbf{E}_L \perp c$, namely the center line of the triplet. Oscillators at IIIa, and IIIb are different with respect to the rotation of the octahedra indeed, but within the experimental linewidth only one line is observed. A nonstatistical distribution of hydrogen can be excluded, because of an almost equal intensity of the lines ν_A, ν_B, and ν_C, when polarized spectra are considered. In the octahedron model we assign the sites I and II to ν_A or ν_C, and IIIa and IIIb are considered to be equal and produce ν_B.

Very similar conclusions can be drawn considering the cube face model. The sites I and II are again inequivalent and different from III. They are assigned to the outer

components and can explain the observed polarized spectra, because of their projection angles between $\mathbf{E}_L$ and the dipole axes. Site III and that created by a rotation of 90° about the c axis are equivalent and are only weakly influenced by the phase transition. Therefore the central peak of the triplet should be assigned to this site, because of its strong polarization with $\mathbf{E}_L \perp c$ and its temperature dependence analogous to that of the volume.

Both models propose 24 sites for hydrogen. In both models the oxygen-hydrogen bonds are along a ⟨110⟩ direction. Thus the set of dipole directions is identical in both models. Consequently, as far as only the directions of the dipoles are concerned, the predictions of the splitting pattern due to external fields are the same. A decision between the different models must be based on properties, which reflect the different neighborhood of the sites. This will be discussed in more detail after a presentation of the influence of external fields on the stretching vibration.

B. Stress dependence

External fields can serve as an experimental tool to collect more information on the hydrogen sites responsible for a certain optical transition. We start with uniaxial stress in [100] direction. Figure 7 shows the results obtained at $T=4.2$ K for various directions of the propagation and polarization of the light beam (for details consult the insert). The bottom spectrum of Fig. 7 is that for zero stress and light polarization $\mathbf{E}_{L2}\|[010]$. The three spectra above are measured with an uniaxial stress $S=174$ N mm^{-2} along [100]. For stress S_{100}, tetragonal c axes are allowed along the y and z axis, respectively. The sample is not monodomain, but has [010] domains. The ratio of these domains can be read off from the absorption peak ν_B from the spectra with $\mathbf{E}_{L2}\|[010]$ and $\mathbf{E}_{L3}\|[001]$. A preferential alignment of the tetragonal c axis along [001] was found, and has been taken into account for the conclusions drawn below. The components ν_A and ν_C split into doublets, while ν_B only shifts to lower energies. Both peaks of the doublet are seen for $\mathbf{E}_{L3}\|[001]$, while $\mathbf{E}_{L2}\|[010]$ produces the low-energy peak of the doublet and $\mathbf{E}_{L1}\|[100]$ the high-energy one. The splitting can be explained as follows. Because ν_A and ν_C are related to the sites I and II, one half of the dipoles is aligned perpendicular to the uniaxial stress, while the other half makes an angle of 45° with S. The sites III are equivalent with respect to S and thus show no splitting. Each light polarization, $\mathbf{E}_{L1}$ or $\mathbf{E}_{L2}$ is perpendicular to one set of dipoles and has a nonzero angle with the members of the other set. For $\mathbf{E}_{L3}$ both sets form nonzero scalar products with the dipole axes. The stress dependence of the components ν_A, ν_B, and ν_C is different, resulting in a splitting ν_C-ν_A increasing linearly with S.[38] In addition the splitting is larger for light polarization perpendicular to S than for a parallel configuration. This behavior can be explained by an increase of the rotation of the octahedra under uniaxial stress[42] and an additional distortion of the octahedra.

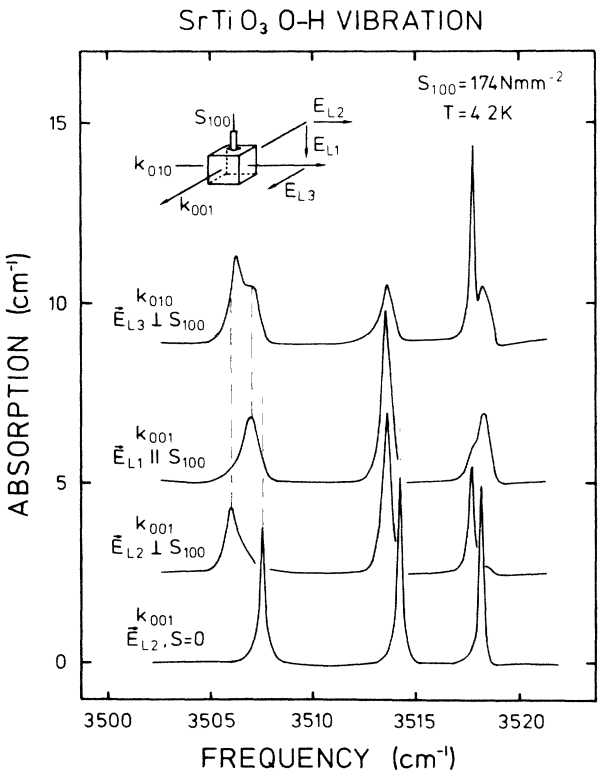

FIG. 7. O-H stretching vibration in $SrTiO_3$ under uniaxial stress along [100]. The spectra are shifted for better viewing.

For these experiments with uniaxial stress along [110] samples with both hydrogen and deuterium doping have been used. With S_{110} stress a monodomain sample with the tetragonal c axis along [001] was produced. This axis served as the propagating direction of the light, too. Figure 8 shows the results of S_{110} stress at helium temperature. In all these cases a shift to lower energies is observed, but of different size for the three components. The shifts, linear in S_{110}, are strongest for ν_A and almost negligible for ν_C. For both ν_A and ν_C no individual splitting with stress is predicted, because in monodomain samples all sites of type I and II make an angle of 60° with the stress direction. However, the sites of type III have different angles with S. One half of them is parallel to S_{110}, while the other half is perpendicular. The splitting proposed by both models for ν_B could not be verified within the half-width of the line.

C. Electric field dependence

An external static electric field offers another possibility to decide between dipole sites. Under electric field dipoles aligned parallel or antiparallel with respect to E are no longer equivalent, as has been outlined in Eq. (3.10).

Before we go into the details of the electric field splitting, we want to mention two effects, which are responsible for a general shift of the bands. First, we applied to each sample an uniaxial stress of 51 N mm^2 along the [110] direction in order to assure the crystals to be monodomain below T_0. This corresponds to a relative shift of ν_A and ν_B of less than 10^{-4}, which is in the order of the half-width. Second, a volume change is caused by the induced polarization, because of electrostriction.[43] The increase of the volume shifts the oscillators to lower ener-

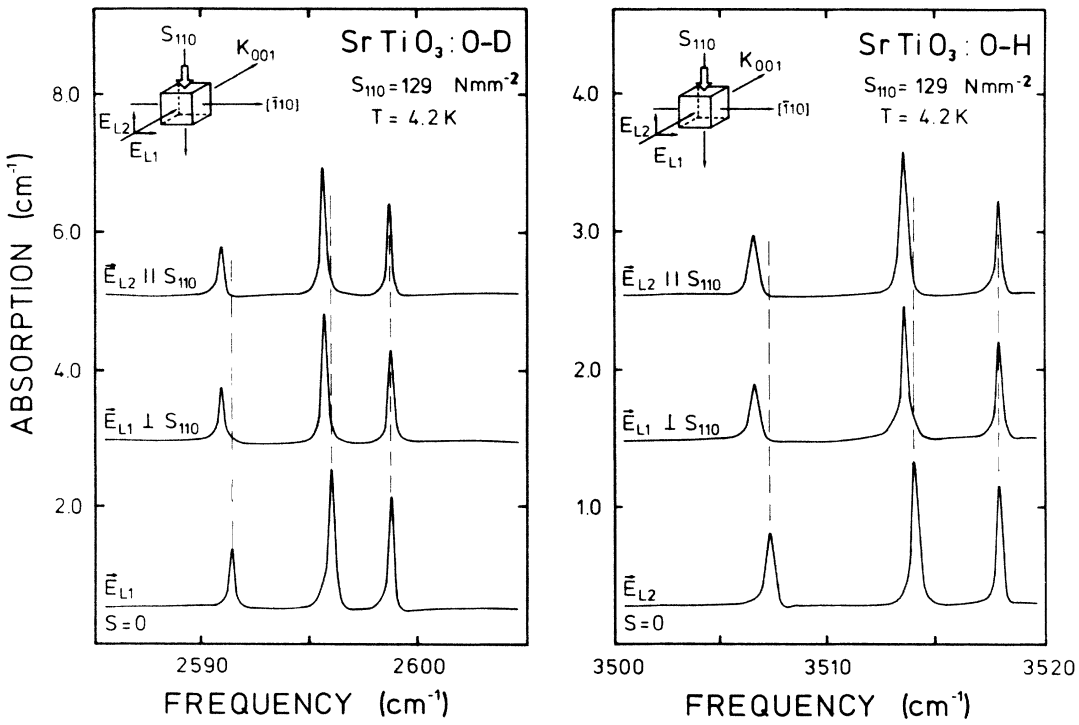

FIG. 8. Absorption spectra of the O-H and O-D stretching vibrations under uniaxial stress S_{110}.

gies in analogy to the temperature dependence.

Uniaxial stress along [110] produces monodomain samples with the tetragonal c axis along [001]. For the electric field E we used the configurations $\mathbf{E}||[001]$ and $\mathbf{E}||[110]$. In each case the propagation of light was chosen perpendicular to E in order to be able to measure the spectra with $\mathbf{E}_L \perp \mathbf{E}$ and $\mathbf{E}_L||\mathbf{E}$. Figure 9 shows the spectra for $\mathbf{E}||[001]$ for a sample containing both hydrogen and deuterium. Under both polarizations of the light beam, the outer components ν_A and ν_C split into a doub-

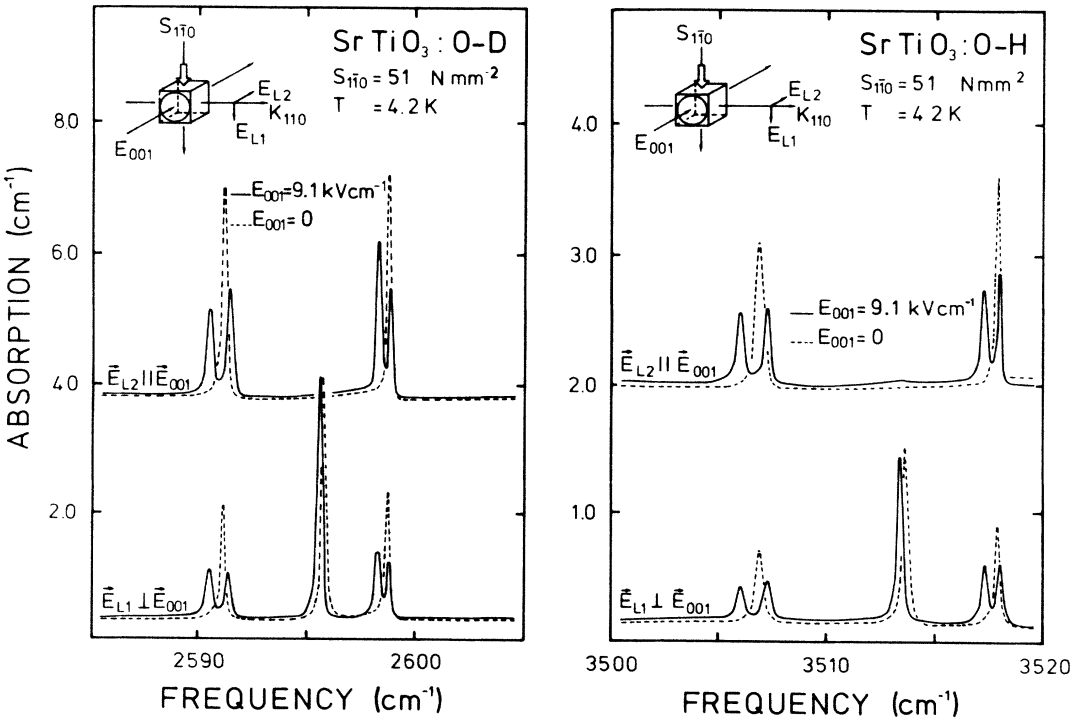

FIG. 9. Stretching vibrations of monodomain $SrTiO_3$:H(D) under electric field E_{001} along the tetragonal axis.

let, while the center line remains a singlet (for $\mathbf{E}_L||[110]$ only). The dipoles of the sites of type I and II, responsible for ν_A, ν_C form an angle of 45° with E, predicting a splitting. The larger splitting of ν_A compared with ν_C should be kept in mind for the further discussion. The dipoles corresponding to the center line ν_B are perpendicular to E and thus do not split. The observed general shift of the spectrum is due to the electrostriction as already mentioned.

Results obtained for $\mathbf{E}||[110]$ are presented in Fig. 10. Again we have an overall shift to lower energies and a splitting of the outer components. But in contrast to the case ($\mathbf{E}||[001]$) just discussed, the size of the splitting here is equal for ν_A and ν_C. The center line ν_B remains a single line for $\mathbf{E}_{L1}||[110]$, but forms a doublet for $\mathbf{E}_{L2}||[110]$. The size of this splitting is twice that of the outer components. The explanation of this result goes along the following lines. First we notice, that dipoles of type I and II form an angle of 60° with the field E_{110}. Thus an equal splitting for ν_A and ν_C is predicted and observed. One half of the type III dipoles is parallel the other half is perpendicular to E_{110}. Those dipoles, which are perpendicular to the electric field, are not affected by the field, and therefore do not show any splitting. On the other hand, those which are parallel show a splitting, which is twice that of ν_A, and ν_C, because of a difference of a factor $\cos 60° = \frac{1}{2}$ in the corresponding scalar products of the potential energy.

In order to draw more stringent conclusions we investigated an additional direction of the field, namely the $\mathbf{E}||[100]$ case. A small uniaxial stress of $S_{100} = 28$ N mm^{-2}, producing a line shift and splitting less than the half-width, was applied to an appropriate crystal containing hydrogen. Domains with the c axis along [010] or [001] result, as already explained in the preceding section for the case of S_{100} stress. The parallel alignment of S_{100} and E_{100} insures a perpendicular orientation of the electric field E_{100} with respect to the tetragonal axes along a or b in the two different domains of the crystal. Figure 11 shows the results for different propagations and polarizations of the light. The height of the band ν_B for zero (broken lines) indicate a preferential alignment of the tetragonal axis along [010]. The spectrum at the bottom of Fig. 11 was taken with light propagating along [001] and polarization $\mathbf{E}_{L2}||[010] \perp \mathbf{E}_{100}$. The upper two spectra are observed with light propagating along [010] and light polarization parallel or perpendicular to E_{100}. The center line ν_B splits into a doublet with equal spacing in all three cases investigated. The same splitting pattern was found for $\mathbf{E}_{L1}||[100]||\mathbf{E}_{100}$ for the outer components ν_A, ν_C. Triplets may be deduced for configurations with the polarization of the light perpendicular to the static field. The triplet can be seen clearly for ν_C but is hardly resolved in the case of ν_A. The splitting pattern, in particular the occurrence of a triplet, follows immediately from the set of oscillators proposed. All dipoles of type III and one half of those of type I and II form an angle of 45° with the field. Light with polarization vector parallel [100] interacts with all these dipoles in the same manner. This explains the equal splitting patterns in the upper spectrum of Fig. 11. The other half of type I and II dipoles are perpendicular to E_{100}. For light with $\mathbf{E}_L \perp [100]$ this half of dipoles is seen, too. In this case no splitting is predicted and observed, because these dipoles are perpendicular to E_{100}. Summing up a pattern of three lines results for the outer components.

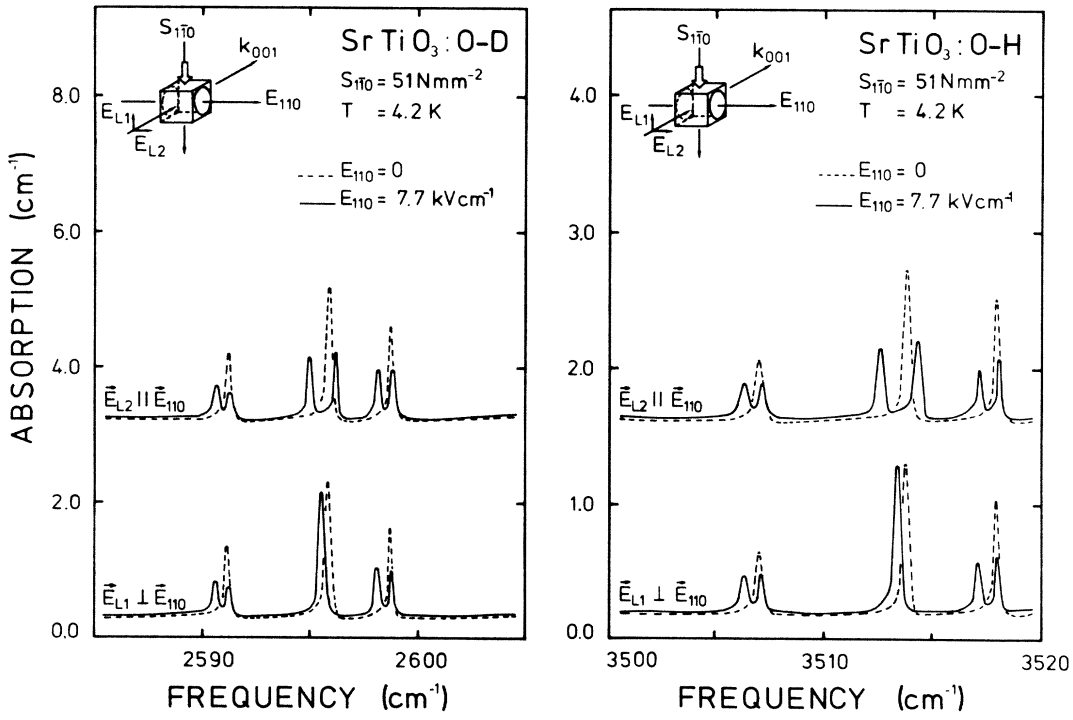

FIG. 10. Stretching vibrations of monodomain $SrTiO_3$:H(D) under electric field E_{110} perpendicular to the tetragonal axis.

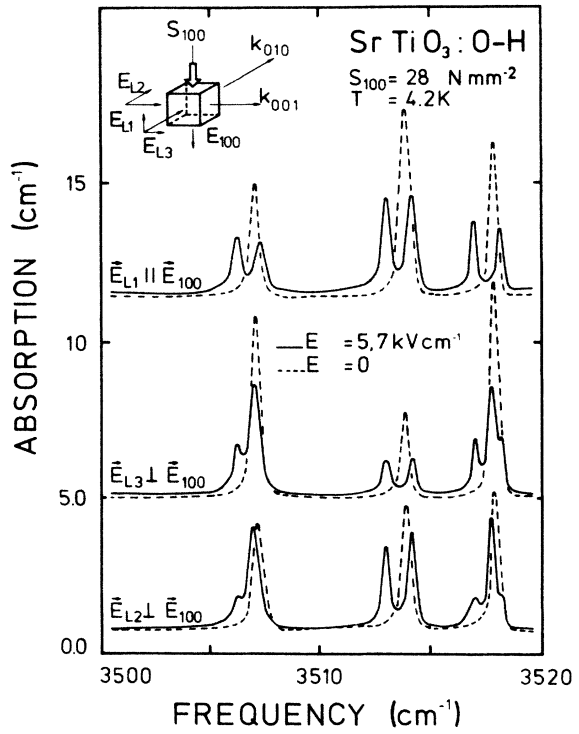

FIG. 11. Stretching vibration of $SrTiO_3$:H under electric field E_{100} perpendicular to the tetragonal axis.

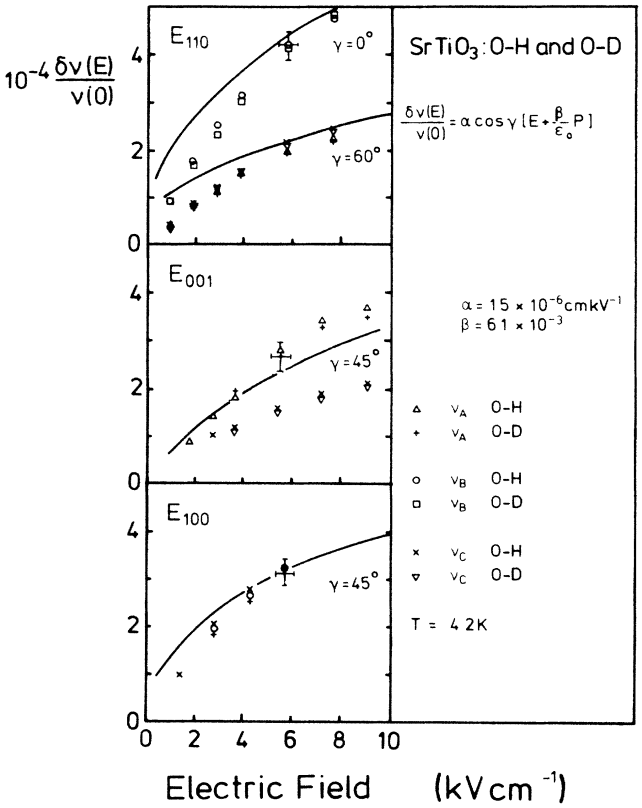

FIG. 12. The relative splitting of the stretching vibrations in $SrTiO_3$H(D) for different electric field directions.

Hysteresis effects impede a quantitative analysis of the field splitting. For the evaluation the full hysteresis curves have been measured in the following way. First the static field was raised in several steps up to a maximum and then lowered. For each step a spectrum was recorded. After a reversal of the electric field the procedure was repeated in order to obtain the complete hysteresis curve. Finally the mean splitting at each field strength was determined and plotted in Fig. 12 for the three different orientations of E. For an easy comparison of results for hydrogen and deuterium, the relative quantity $\delta\nu(E)/\nu(0)$ was chosen. The lines in Fig. 12 have been calculated with Eq. (3.10) according to

$$\frac{\delta\nu}{\nu}(E)=\alpha E_{\rm loc}\cos\gamma=\alpha\left[E+\frac{\beta}{\varepsilon_0}P\right]\cos\gamma\ . \tag{4.1}$$

The local field $E_{\rm loc}$ acting upon an anharmonic oscillator was taken in the Lorentz approximation

$$E_{\rm loc}=E+\frac{\beta}{\varepsilon_0}P\ . \tag{4.2}$$

E is the applied electric field, P the field-induced polarization, β the Lorentz factor, ε_0 the permittivity of free space, and γ describes the angle between the dipoles and the field E. The quantities α,β,P are determined as follows. The parameter α can be calculated from spectroscopic data according to Eq. (3.11). Using the data for ν_B at 4.2 K we obtain $\alpha=1.5\times10^{-6}$ cm/kV.

The field-induced polarization P has been derived from the minimum of the derivative of the free energy with respect to P according to

$$\chi P+\xi P^3-E=0\ . \tag{4.3}$$

Here χ is the dielectric inverse susceptibility, which is almost identical with the reciprocal dielectric constant. The parameter ξ has been determined from electric field dependent measurements of the dielectric constant[44,45] to be $\xi=6.5\times10^{16}$ kV cm$^5C^{-3}$ independent of the temperature. Taking the inverse susceptibility of Ref. 46, Eq. (4.3) allows the calculation of $P(E,T)$. The parameter β follows from the splitting of one component at a given field E. With $\delta\nu$ at $E_{110}=7.7$ kV cm^{-1} we obtained $\beta=6.2\times10^{-3}$. The curves, calculated with these parameters, describe the experimental data in a very reasonable way, except for ν_C in the case of a E_{001} field.

The field-induced polarization $P(E,T)$ depends on the temperature, as mentioned above. Due to the temperature dependence of $\chi(T)$, the polarization $P(E,T)$ decreases with increasing temperature. The nonlinear dependence of P on E at helium temperature changes to a linear relation at liquid-nitrogen temperature. Thus a linear increase of $\delta\nu_B$ with E is expected and in fact observed at 86 K.[38] The temperature dependence of $\delta\nu_B$ at a fixed field is given in Fig. 13 together with a corresponding calculation using the parameter set given above. The trend is well reproduced, but the quantitative agreement is poor. The deviation is more pronounced at higher temperatures, which might reflect the influence of the soft mode on P, which has been neglected in our calculations.

A numerical analysis of Eq. (4.1) shows, that the split-

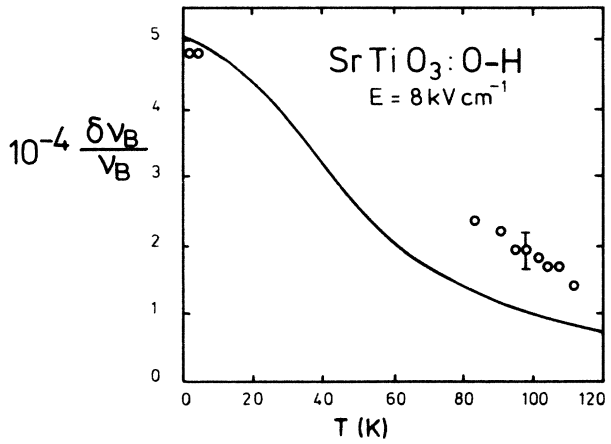

FIG. 13. Temperature dependence of the splitting of transition ν_B under constant electric field along [110].

ting $\delta\nu/\nu$ is mainly determined by the second term, which is proportional to the product of α and β. Therefore similar or even improved fits are obtainable with other parameter sets, as far as the produced $\alpha\cdot\beta$ is not altered very strongly. Since α is given by the evaluation of the spectroscopic parameters, one might use Eq. (4.1) to deduce a phenomenological value of β for the local field correction. In view of the simplified model used, this value, however, should not be taken to be accurate. The feedback parameter $\beta=4.5\times10^{-4}$ given in the literature[47] according to a Curie-Weiss–type behavior, is even smaller than our value rather than a Lorentz factor $\frac{1}{3}$, indicating the difficulties encountered in applying the local field correction.

V. DISCUSSION

The octahedron model and the cube face model consist of sets of dipoles, which are equivalent with respect to the orientation of the dipolar axes. Thus simple geometrical arguments for the dipoles and their splitting pattern under external perturbations yield the same predictions for both models. The situation changes if the site symmetry of the dipoles and the size of the splitting pattern is considered. In Fig. 12 we have demonstrated that Eq. (4.1), using an isotropic Lorentz factor β, can describe the electric field splitting for E_{110} and E_{100} in an almost quantitative manner. This agreement is not found for E_{001}. Here the splitting of ν_A follows Eq. (4.1) with acceptable deviations, but ν_C shows a splitting of approximately one half of the predicted value. On the other hand, since the transitions ν_A and ν_C behave identically in all other cases investigated, we have to assume equal orientations of the vibrations. This discrepancy can be solved if different local fields for the oxygen ions involved are considered. In the cube face model, both ν_A and ν_C are related to the same O_b^{2-} oxygen ion (Fig. 6) and one has to expect therefore the same splitting factors for ν_A and ν_C. The octahedron model, on the other hand, relates one band with the O_a ion and the other with the O_b ion (Fig. 6). These are different ions with respect to site symmetry. Different Lorentz factors are easily justified in accordance with theoretical calculations by Slater.[48] The experimental result of different splitting factor for ν_A and ν_C therefore supports the octahedron model.

The temperature dependence of the stretching vibrations at the phase transition offers an additional argument in favor of the octahedron model. The high frequency line ν_C deviates only weakly from a linear extrapolation of the temperature dependence in the cubic phase.[21,22,24,38] Therefore this dipole should be generated by a hydrogen ion linked to an O_a ion, which is only weakly influenced by the phase transition. In contrast to line ν_C, the line ν_A is subject to a strong deviation from a linear extrapolation. A H—O_b bond fulfills this requirement. Therefore the octahedron model explains this behavior without any problem. The cube face model would predict an almost equal temperature dependence for ν_A and ν_C, in contrast to the experimental finding. Our conclusion that the lines ν_A and ν_C should be related to H sites at different oxygen ions is supported by the significant difference in their spectroscopic constants at helium temperature, compare Table II.

Hydrogen bound to oxygen has been investigated in many other oxidic materials, such as $KTaO_3$,[18] TiO_2,[13,14,49] $LiNbO_3$,[50] SiO_2,[7,51] Al_2O_3,[17] and $Ba_2NaNb_5O_{15}$.[52] None of the investigations just cited propose a proton vibrating in the direction of a positive ion. A calculation of the potential energy is available for TiO_2.[48] The minima are found in the direction of an adjacent oxygen ion. These results and our own investigations of $BaTiO_3$ (Ref. 40) support a hydrogen site in between two adjacent oxygen ions. A recent calculation[53] for hydrogen in $SrTiO_3$ indeed shows sites of minimum energy in direction of oxygen-oxygen connections of the octahedra in $SrTiO_3$.

ACKNOWLEDGMENTS

We are indebted to Dr. H. Hesse of the crystal growth laboratory of the University of Osnabrück for supplying and preparing some of the crystals used. The assistance of D. Noeske with the Fourier ir measurements is gratefully acknowledged. The authors are grateful to V. Gericke and A. Jovanović for part of the Raman measurements and to A. Förster for the ir study of the O-D overtone stretching vibration. We thank the Deutsche Forschungsgemeinschaft for financial support (Sonderforschungsbereich 225/C1, Oxidische Kristalle).

*Author to whom correspondence should be directed.

[1]J. Jackel, A. M. Glass, G. E. Peterson, C. E. Rice, D. H. Olson, and J. J. Veselka, J. Appl. Phys. 55, 269 (1984).
[2]M. De Micheli, J. Botineau, P. Sibillot, D. B. Ostrowsky, and M. Papuchon, Opt. Commun. 42, 101 (1983).
[3]H. Vormann, G. Weber, S. Kapphan, and E. Krätzig, Solid State Commun. 40, 543 (1981).
[4]R. G. Smith, D. B. Fraser, R. T. Denton, and T. C. Rich, J.

Appl. Phys. **39**, 4600 (1968).
[5]W. A. Phillips, Philos. Mag. B **43**, 747 (1981).
[6]B. Subramaniam, L. E. Halliburton, and J. J. Martin, J. Phys. Chem. Solids **45**, 575 (1984).
[7]F. L. Galeener and J. C. Mikkelsen, Jr., Appl. Phys. Lett. **38**, 336 (1981).
[8]M. Horiguchi and M. Kawachi, Appl. Optics **17**, 2570 (1978).
[9]W. Radloff, E. Below, H. Wagner, and P. Kleinert, Phys. Status Solidi A **69**, K21 (1982).
[10]W. M. Theis, G. B. Norris, and M. D. Porter, Appl. Phys. Lett. **46**, 1033 (1985).
[11]Y. Chen, R. Gonzalez, O. E. Schow, and G. P. Summers, Phys. Rev. B **27**, 1276 (1983).
[12]G. P. Summers, T. M. Wilson, B. T. Jeffries, H. T. Tohver, Y. Chen, and M. M. Abraham, Phys. Rev. B **27**, 1283 (1983).
[13]O. W. Johnson, J. DeFord, and J. W. Shaner, J. Appl. Phys. **44**, 3008 (1973).
[14]J. B. Bates and R. A. Perkins, Phys. Rev. B **16**, 3713 (1977).
[15]Y. Chen, R. Gonzalez, and K. L. Tsang, Phys. Rev. Lett. **53**, 1077 (1984).
[16]R. Gonzalez, Y. Chen, K. L. Tsang, and G. P. Summers, Appl. Phys. Lett. **41**, 739 (1982).
[17]H. Engstrom, J. B. Bates, J. C. Wang, and M. M. Abraham, Phys. Rev. B **21**, 1520 (1980).
[18]H. Engstrom, J. B. Bates, and L. A. Boatner, J. Chem. Phys. **73**, 1073 (1980).
[19]R. Gonzalez, M. M. Abraham, L. A. Boatner, and Y. Chen, J. Chem. Phys. **78**, 660 (1983).
[20]F. G. Wakim, J. Chem. Phys. **49**, 3738 (1968).
[21]A. F. W. Klukhuhn, J. Bruining, B. Klootwijk, and J. van der Elsken, Phys. Rev. Lett. **25**, 380 (1970).
[22]S. Kapphan, J. Koppitz, and G. Weber, Ferroelectrics **25**, 585 (1980).
[23]J. L. Brebner, S. Jandl, and Y. Lepine, Phys. Rev. B **23**, 3816 (1981).
[24]S. Jandl, D. Houde, Y. Lepine, and J. L. Brebner, Ferroelectrics **38**, 805 (1981).
[25]Crystals grown by the Verneuil method are from (a) Nakazumi Crystal. Corp., 2-1, Sakae-machi, Ikeda-shi, Osaka, Japan, (b) Commercial Crystal Laboratories Inc., 111 Chevalier Ave. South Amboy, New Jersey 08879, USA.
[26]Crystals grown by the Czochralski method are from Dr. H. Hesse, Crystal Laboratory, University of Osnabrück.
[27]H. Hesse and S. Kapphan, Phys. Status Solidi A **50**, K243 (1978).
[28]S. Kapphan and F. Lüty, J. Phys. Chem. Solids **34**, 969 (1973).
[29]R. V. Jimenez and F. Lüty, Phys. Rev. B **12**, 1531 (1974).
[30]B. Wedding and M. V. Klein, Phys. Rev. **177**, 1274 (1969).
[31]H. S. Heaps and G. Herzberg, Z. Phys. **133**, 48 (1952).
[32]P. E. Cade, J. Chem. Phys. **47**, 2390 (1967).
[33]K. A. Müller, W. Berlinger, and F. Waldner, Phys. Rev. Lett. **21**, 814 (1968).
[34]K. A. Müller and W. Berlinger, Phys. Rev. Lett. **26**, 13 (1971).
[35]K. A. Müller, W. Berlinger, M. Capizzi, and H. Gränicher, Solid State Commun. **8**, 549 (1970).
[36]M. Tinkham, *Group Theory and Quantum Mechanics* (McGraw-Hill, New York, 1964).
[37]G. Herzberg, *Molecular Spectra and Molecular Structure I. Spectra of Diatomic Molecules* (van Nostrand, Princeton, N.J., 1950).
[38]G. Weber, Dissertation, University of Osnabrück, 1982 (unpublished).
[39]M. Wöhlecke, and S. Kapphan (unpublished).
[40]J. C. Owrutsky, N. H. Rosenbaum, L. M. Tack, and R. J. Saykally, J. Chem. Phys. **83**, 5338 (1985).
[41]S. Kapphan and G. Weber, Ferroelectrics **37**, 673 (1981).
[42]H. Uwe and T. Sakudo, Phys. Rev. B **13**, 271 (1976).
[43]G. Schmidt and E. Hegenbarth, Phys. Status Solidi **3**, 329 (1963).
[44]E. Hegenbarth, Phys. Status Solidi **6**, 333 (1964).
[45]M. A. Saifi and L. E. Cross, Phys. Rev. B **2**, 677 (1970).
[46]T. Sakudo and H. Unoki, Phys. Rev. Lett. **26**, 851 (1971).
[47]A. R. v. Hippel, J. Phys. Soc. Jpn. Suppl. **28**, 1 (1970).
[48]J. C. Slater, Phys. Rev. **78**, 748 (1950).
[49]J. B. Bates, J. C. Wang, and R. A. Perkins, Phys. Rev. B **19**, 4130 (1979).
[50]J. R. Herrington, B. Dischler, A. Räuber, and J. Schneider, Solid State Commun. **12**, 351 (1973).
[51]F. Porreca, Solid State Commun. **7**, 961 (1969).
[52]L. C. Bobb, J. Lefkowitz, and L. Muldawer, Solid State Commun. **7**, 937 (1969).
[53]C. R. A. Catlow (private communication).